

The universal Higgs fit

Pier Paolo Giardino^{a,b}, Kristjan Kannike^{c,d},
Isabella Masina^{e,f}, Martti Raidal^{d,g} and Alessandro Strumia^{a,d}

(a) *Dipartimento di Fisica, Università di Pisa and INFN, Italy*

(b) *CERN, Theory Division, CH-1211 Geneva 23, Switzerland*

(c) *Scuola Normale Superiore and INFN, Piazza dei Cavalieri 7, 56126 Pisa, Italy*

(d) *National Institute of Chemical Physics and Biophysics, R  vala 10, Tallinn, Estonia*

(e) *Dipartimento di Fisica e Scienze della Terra dell'Universit   di Ferrara and INFN, Italy*

(f) *CP  -Origins and DIAS, Southern Denmark University, Denmark*

(g) *Institute of Physics, University of Tartu, Estonia*

Abstract

We perform a state-of-the-art global fit to all Higgs data. We synthesise them into a ‘universal’ form, which allows to easily test any desired model. We apply the proposed methodology to extract from data the Higgs branching ratios, production cross sections, couplings and to analyse composite Higgs models, models with extra Higgs doublets, supersymmetry, extra particles in the loops, anomalous top couplings, invisible Higgs decay into Dark Matter. Best fit regions lie around the Standard Model predictions and are well approximated by our ‘universal’ fit. Latest data exclude the dilaton as an alternative to the Higgs, and disfavour fits with negative Yukawa couplings. We derive for the first time the SM Higgs boson mass from the measured rates, rather than from the peak positions, obtaining $M_h = 124.2 \pm 1.8 \text{ GeV}$.

1 Introduction

After the discovery of a new particle around 125.5 GeV announced by the ATLAS [1] and CMS [2] LHC collaborations during 2012, all LHC and TeVatron collaborations presented at the Moriond 2013 conference the new results based on the full collected data. These include the most important $\gamma\gamma$, ZZ^* and WW^* channels as well as updates to the fermionic channels. Such results will stay with us for next two years until LHC with full energy starts operating. Therefore it is the right moment to analyse their implications.

We want to know if the new particle is the long-awaited Standard Model (SM) Higgs boson [3, 4, 5, 6]. On one side, the experimental collaborations are measuring its discrete quantum numbers to check if it is a scalar. On the other side, various theoretical groups [7, 8, 9] started to approximatively reconstruct from data its production cross section and its decay modes and consequently its couplings to check if they agree with the SM predictions or with other models beyond the SM. Clearly, this is a more significant test that can be precisely done only by the experimental collaborations, which indeed started to present analyses along these lines. However these experimental fits, presented in the form of likelihood plots within a few specific beyond-the-SM models, are of little use to theorists who are interested in different models.

We here propose how experimental collaborations could report their results in a model-independent and useful way, such that these results would be readily and reliably used by theorists who want to test any desired model. The new ingredient that we introduce and that allows for this simplification is the assumption that new physics can be approximated as a first-order perturbation with respect to the SM predictions. We find that this assumption is increasingly supported by data, that agree with the SM with precisions around the 20% level.

Such results, obtained after two years of LHC operation and with only 25/fb data per experiment, implies severe constraints on models where the Higgs boson is a portal to new physics. We analyse several models and rule out alternative scenarios to the Higgs boson.

The paper is organised as follows. In section 2 we present the data and our fitting procedure. In section 3 we derive the first measurement of the Higgs mass from the rates, rather than from the position of the peaks in the $\gamma\gamma$ and ZZ invariant mass distributions. In section 4 we present the ‘universal’ format for data mentioned above. Next, in section 5 we present fits in various specific models, updating our previous results and comparing the full fit to the simplified ‘universal’ fit to verify that it is a good approximation. We fit Higgs cross sections in section 5.1, Higgs couplings in 5.2, composite Higgs models in 5.3, new physics in loops in 5.4, two Higgs doublet models in 5.5, the MSSM in 5.6, the dilaton in 5.7, the Higgs invisible width in 5.8 and models where DM couples to the Higgs in 5.9. In section 6 we summarise the results and draw our conclusions.

2 The data

Searches for the SM Higgs boson have been carried out in proton-proton collisions at $\sqrt{s} = 7$ (2011 data) and 8 TeV (2012 data) with about 25/fb of total integrated luminosity.

There are four main production modes for Higgs boson from pp collisions at $\sqrt{s} \sim 8$ TeV. The gluon-gluon fusion production mode has the largest cross section, followed in turn by vector boson fusion (VBF), associated Wh and Zh production, and production in association with top quarks, $t\bar{t}h$. The cross sections for the Higgs boson production modes and the decay branching fractions, together with their uncertainties, are taken from [10].

Our updated analysis uses the new data presented at the Moriond 2013 conference by the CMS, ATLAS and TeVatron collaborations [11, 12, 13, 14] in the following five decay modes: $\gamma\gamma$ [15], ZZ^* (followed by ZZ^* decays to $4\ell, 2\ell 2\nu, 2\ell 2q, 2\ell 2\tau$) [16], WW^* (followed by WW^* decays to $\ell\nu\ell\nu, \ell\nu qq$) [17, 12], $\tau^+\tau^-$ (followed by leptonic and hadronic decays of the τ -leptons) [13, 18] and $b\bar{b}$ [13, 19], and the first tentative measurements in the $\mu^+\mu^-$ [20] and $Z\gamma$ channels [21], as well as their combination [22]. Here and throughout, ℓ stands for electrons or muons and q for quarks.

For a given Higgs boson mass, the search sensitivity depends on the production cross section of the Higgs boson, its decay branching fraction into the chosen final state, the signal selection efficiency, the mass resolution, and the level of standard model backgrounds in the same or a similar final state. For low values of the Higgs boson mass, the $h \rightarrow \gamma\gamma$ and $h \rightarrow ZZ^* \rightarrow 4\ell$ channels play a special role due to the excellent mass resolution for the reconstructed diphoton and four-lepton final states, respectively. The $h \rightarrow WW^* \rightarrow \ell\nu\ell\nu$ channel provides high sensitivity but has relatively poor mass resolution due to the presence of neutrinos in the final state. The sensitivity in the $b\bar{b}$ and $\tau^+\tau^-$ decay modes is reduced due to the large backgrounds and poor mass resolutions.

We include in our data-set all exclusive $\gamma\gamma$ and $\tau\tau$ sub-categories described by the experimental collaborations by telling how much each Higgs production channel in the SM contributes to the various rates. We adopt the MultiVariate Analysis (MVA) $\gamma\gamma$ analysis from CMS and we combine all experiments, such that we find an average $\gamma\gamma$ rate very close to the SM prediction. Consequently our results differ from previous analyses performed without including the latest CMS $\gamma\gamma$ data [7].

This is an important issue because, while most of the presented LHC results are well consistent with the SM predictions within experimental errors, there are few unexpected new developments that need commenting. The most important of them is the discrepancy between the ATLAS and CMS results in the $h \rightarrow \gamma\gamma$ channels. With full luminosity, ATLAS finds an overall rate of 1.65 ± 0.34 , higher than the SM prediction of 1, and higher than the CMS result of 0.80 ± 0.30 . The two measurements are compatible within 2σ . In addition, the two CMS $\gamma\gamma$ analyses (MVA and cut based) show different signal rates. Finally, the two Higgs boson mass determinations in ATLAS, from the peaks in the $\gamma\gamma$ and ZZ channels, differ by 2σ . Both experiments have cross checked their analyses and reached conclusions that those deviations are due to statistical fluctuations of both signal and background. This conclusion implies that: (i) combining all data in a global fit is meaningful and increases the precision; (ii) selecting instead any single measurement, for example the ATLAS excess in $\gamma\gamma$, is not justified and introduces a bias in the data.

The experimental collaborations report Higgs boson rates R in units of the central value

and marginalising it with respect to the free parameters σ_j , constrained to have a central value σ_j^{th} and an uncertainty σ_j^{err} given by

$$\begin{aligned} \sigma(pp \rightarrow h)_{\text{th}} &= (19.4 \pm 2.8) \text{ pb}, & \sigma(pp \rightarrow jjh)_{\text{th}} &= (1.55 \pm 0.04) \text{ pb}, \\ \sigma(pp \rightarrow Wh)_{\text{th}} &= (0.68 \pm 0.03) \text{ pb}, & \sigma(pp \rightarrow Zh)_{\text{th}} &= (0.39 \pm 0.02) \text{ pb}, \\ \sigma(pp \rightarrow t\bar{t}h)_{\text{th}} &= (0.128 \pm 0.018) \text{ pb} & & \text{at } \sqrt{s} = 8 \text{ TeV}. \end{aligned} \quad (3)$$

We summarise all data in fig. 1 together with their 1σ error-bars. The grey band shows the $\pm 1\sigma$ range for the average of all rates: 1.00 ± 0.10 . It lies along the SM prediction of 1 (horizontal green line) and is about 10σ away from 0 (the horizontal red line is the background-only rate expected in the absence of a Higgs boson).

3 Reconstructing the Higgs mass

The CMS and ATLAS collaborations reported measurements of the pole Higgs mass M_h obtained as the position of the peaks observed in the invariant mass of the $h \rightarrow \gamma\gamma$ and $h \rightarrow ZZ \rightarrow 4\ell$ distributions:

$$M_h = 125.66 \pm 0.34 \text{ GeV} = \begin{cases} 125.4 \pm 0.5_{\text{stat}} \pm 0.6_{\text{syst}} \text{ GeV} & \text{CMS } \gamma\gamma \\ 125.8 \pm 0.5_{\text{stat}} \pm 0.2_{\text{syst}} \text{ GeV} & \text{CMS } ZZ \\ 126.8 \pm 0.2_{\text{stat}} \pm 0.7_{\text{syst}} \text{ GeV} & \text{ATLAS } \gamma\gamma \\ 124.3 \pm 0.6_{\text{stat}} \pm 0.5_{\text{syst}} \text{ GeV} & \text{ATLAS } ZZ \end{cases}. \quad (4)$$

These measurements are mutually compatible, and the uncertainty is so small that in the subsequent fits to rates we can fix M_h to its combined best-fit value.

Indeed, we here discuss how the Higgs mass can be independently measured, with a bigger uncertainty, by requiring that the measured rates agree with their SM predictions. Such predictions have a dependence on the Higgs mass that, around 125 GeV, can be approximated as

$$\sigma(pp \rightarrow X) \approx \sigma(pp \rightarrow X)_{M_h=125 \text{ GeV}} \times [1 + c_X \times (M_h - 125 \text{ GeV})]. \quad (5)$$

In table 1 we list the values of the coefficients c_X and of the measured rates for the various processes averaging all experiments, as well as the Higgs mass indirectly derived from such rates. We see that the single best indirect determination of M_h comes from the $h \rightarrow WW$ rates, that presently have no sensitivity to M_h if one wants to measure it from a mass peak. On the other hand, the $h \rightarrow \gamma\gamma$ signal that offers the best peak measurement of M_h has very little indirect sensitivity to M_h , because the $\gamma\gamma$ rate happens to have a weak dependence on M_h . Averaging over all channels we find

$$M_h = 124.2 \pm 1.8 \text{ GeV} \quad (\text{Higgs mass extracted from the rates, assuming the SM}) \quad (6)$$

which is compatible with the determination of the pole Higgs mass obtained in a model-independent way from the positions of the peaks.

Process X	$h \rightarrow WW$	$h \rightarrow ZZ$	$h \rightarrow \gamma\gamma$	$Vh \rightarrow Vbb$	$h \rightarrow \tau\tau$
Sensitivity c_X	6.4%/ GeV	7.8%/ GeV	-1.5%/ GeV	-5.4%/ GeV	-4.1%/ GeV
Measured rate/SM	0.84 ± 0.17	1.06 ± 0.22	1.07 ± 0.19	1.19 ± 0.42	1.11 ± 0.28
Higgs mass in GeV	123.0 ± 3.0	126.2 ± 2.7	121 ± 12	122 ± 8	123 ± 7

Table 1: *Determinations of the Higgs mass from the rates, assuming the SM.*

4 The universal Higgs fit

We perform the most generic fit in terms of a particle h with couplings to pairs of $t, b, \tau, W, Z, g, \gamma$ equal to $r_t, r_b, r_\tau, r_W, r_Z, r_g, r_\gamma$ in units of the SM Higgs coupling. This means, for example, that the coupling to the top is given by $r_t(m_t/V)h\bar{t}t$, where $r_t = 1$ in the SM and $V = 246$ GeV is the Higgs vacuum expectation value. Similarly, the $h\gamma\gamma$ coupling is assumed to be r_γ times its SM prediction. In the SM this couplings first arises at one loop level. Experiments are starting to probe also the $h\bar{\mu}\mu$ and the $hZ\gamma$ effective couplings, so that also the corresponding r_μ and $r_{Z\gamma}$ parameters will start to be measured. This discussion can be summarized by the following effective Lagrangian:

$$\begin{aligned} \mathcal{L}_h = & r_t \frac{m_t}{V} h\bar{t}t + r_b \frac{m_b}{V} h\bar{b}b + r_\tau \frac{m_\tau}{V} h\bar{\tau}\tau + r_\mu \frac{m_\tau}{V} h\bar{\mu}\mu + r_Z \frac{M_Z^2}{V} hZ_\mu^2 + r_W \frac{2M_W^2}{V} hW_\mu^+ W_\mu^- + \\ & + r_\gamma c_{\text{SM}}^{\gamma\gamma} \frac{\alpha}{\pi V} hF_{\mu\nu} F_{\mu\nu} + r_g c_{\text{SM}}^{gg} \frac{\alpha_s}{12\pi V} hG_{\mu\nu}^a G_{\mu\nu}^a + r_{Z\gamma} c_{\text{SM}}^{Z\gamma} \frac{\alpha}{\pi V} hF_{\mu\nu} Z_{\mu\nu}. \end{aligned} \quad (7)$$

The various SM loop coefficients c_{SM} are summarised in appendix A. This Lagrangian is often written in a less intuitive but practically equivalent form by either using $\text{SU}(2)_L \otimes \text{U}(1)_Y$ -invariant effective operators, or assuming that the Higgs is the pseudo-Goldstone boson of a spontaneously broken global symmetry and writing its chiral effective theory [7].

Furthermore, we take into account the possibility of Higgs decays into invisible particles X (such as Dark Matter or neutrinos) with branching ratio BR_{inv} . In almost all measured rates BR_{inv} is equivalent to a common reduction r of all the other Higgs couplings, $\text{BR}_{\text{inv}} \simeq 1 - r^2$, such that BR_{inv} is indirectly probed by data [8]. The only observable that directly probes an invisible Higgs width is the $pp \rightarrow Zh \rightarrow \ell^+ \ell^- \bar{X} X$ rate measured by ATLAS [30], which implies

$$\text{BR}_{\text{inv}} = -0.19 \pm 0.43. \quad (8)$$

Any possible new-physics model can be described as specific values of the r_i parameters. Several examples are provided in section 5.

Following the procedure described in the previous section, we approximatively extract from data the function

$$\chi^2(r_t, r_b, r_\tau, r_W, r_Z, r_g, r_\gamma, r_{Z\gamma}, r_\mu, \text{BR}_{\text{inv}}) \quad (9)$$

which describes all the information contained in Higgs data. We find $\chi^2 = 58.8$ at the best fit (56 data points, 10 free parameters), marginally better than the SM fit, $\chi_{\text{SM}}^2 = 61.7$ (no free parameters).

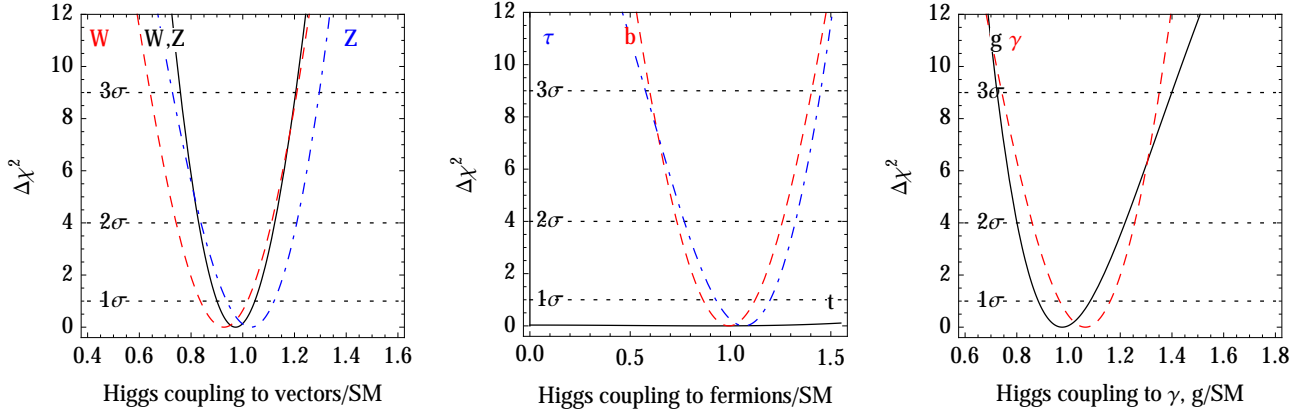


Figure 2: χ^2 as function of the model-independent Higgs couplings r_i to the various SM particles, varying them one-by-one.

4.1 Universal fit to small new physics effects

The universal χ^2 of eq. (9) has a too complicated form to be reported analytically, and depends on too many variables to be reported in numerical form, like plots or tables. For these reasons, previous analyses [7, 8, 9] focused on particular BSM models with a reduced number of parameters. For example, fig. 2 shows the fit as function of each r_i , setting all others to their SM values of unity: we see that the χ^2 are approximately parabolic.

We here observe that Higgs data are converging towards the SM predictions with small errors, thereby it is time to start making the approximation

$$r_i = 1 + \epsilon_i \quad \text{with} \quad \epsilon_i \ll 1 \quad (10)$$

and $\text{BR}_{\text{inv}} = \epsilon_{\text{inv}}$. The observable rates R_I are computed at first order in ϵ_i , and consequently the χ^2 is expanded up to second order in ϵ_i . As well known, this Gaussian approximation is a great simplification; for example marginalizations over nuisance parameters just becomes minimisation, which preserves the Gaussian form. Fig. 2 suggests that this approximation already seems reasonably good.

For LHC at 8 TeV the main observables are approximated as

$$\begin{aligned} R_{h \rightarrow WW} &= 1 - 1.14\epsilon_b + 1.58\epsilon_g - \epsilon_{\text{inv}} - 0.17\epsilon_t + 1.72\epsilon_W + 0.02\epsilon_Z \\ R_{h \rightarrow ZZ} &= 1 - 1.14\epsilon_b + 1.58\epsilon_g - \epsilon_{\text{inv}} - 0.17\epsilon_t - 0.28\epsilon_W + 2.02\epsilon_Z \\ R_{h \rightarrow \tau\tau} &= 1 - 1.14\epsilon_b + 1.58\epsilon_g - \epsilon_{\text{inv}} + 1.83\epsilon_t - 0.28\epsilon_W + 0.02\epsilon_Z \\ R_{h \rightarrow \gamma\gamma} &= 1 - 1.14\epsilon_b + 1.83\epsilon_g - \epsilon_{\text{inv}} - 0.18\epsilon_t - 0.45\epsilon_W - 0.06\epsilon_Z + 2\epsilon_\gamma \\ R_{h \rightarrow bb} &= 1 + 0.86\epsilon_b + 1.58\epsilon_g - \epsilon_{\text{inv}} - 0.17\epsilon_t - 0.28\epsilon_W + 0.02\epsilon_Z \\ R_{V(h \rightarrow bb)} &= 1 + 0.86\epsilon_b - 0.17\epsilon_g - \epsilon_{\text{inv}} - 0.18\epsilon_t + 0.83\epsilon_W + 0.67\epsilon_Z. \end{aligned} \quad (11)$$

The full χ^2 can now be reported in a simple form. Indeed the χ^2 is a quadratic function of the ϵ_i , and it is usually written as

$$\chi^2 = \sum_{i,j} (\epsilon_i - \mu_i) (\sigma^2)_{ij}^{-1} (\epsilon_j - \mu_j), \quad \text{where} \quad (\sigma^2)_{ij} = \sigma_i \rho_{ij} \sigma_j \quad (12)$$

in terms of the mean values μ_i of each parameter ϵ_i , of its error σ_i and in terms of the correlation matrix ρ_{ij} . We believe that this is the most useful form in which experimental collaborations could report their results. From our approximated analysis of LHC and TeVatron data we obtain:

$$\begin{aligned} \epsilon_b &= -0.05 \pm 0.34 \\ \epsilon_g &= -0.21 \pm 0.25 \\ \epsilon_{\text{inv}} &= -0.25 \pm 0.27 \\ \epsilon_W &= -0.09 \pm 0.15 \\ \epsilon_Z &= +0.02 \pm 0.13 \\ \epsilon_\gamma &= +0.02 \pm 0.16 \\ \epsilon_\tau &= +0.03 \pm 0.19 \end{aligned} \quad \rho = \begin{pmatrix} 1 & 0.73 & 0.06 & 0.48 & 0.43 & 0.56 & 0.48 \\ 0.73 & 1 & 0.47 & 0.34 & 0.20 & 0.40 & 0.34 \\ 0.06 & 0.47 & 1 & 0.49 & 0.31 & 0.45 & 0.36 \\ 0.48 & 0.34 & 0.49 & 1 & 0.64 & 0.70 & 0.61 \\ 0.43 & 0.20 & 0.31 & 0.64 & 1 & 0.59 & 0.54 \\ 0.56 & 0.40 & 0.45 & 0.70 & 0.59 & 1 & 0.60 \\ 0.48 & 0.34 & 0.36 & 0.61 & 0.54 & 0.60 & 1 \end{pmatrix}. \quad (13)$$

We have not reported the central value of $r_t = 1 + \epsilon_t$, of $\epsilon_{Z\gamma}$ and of ϵ_μ because they presently are known only up to uncertainties much larger than 1. Future searches for $t\bar{t}h$ production, for $h \rightarrow Z\gamma$ and for $h \rightarrow \mu^+\mu^-$ will improve the situation.

In many models the Higgs couplings to vectors satisfy $\epsilon_W = \epsilon_Z$, because of $\text{SU}(2)_L$ invariance. Furthermore, in many models LEP precision data force ϵ_W and ϵ_Z to be very close to 0. This restriction can of course be implemented by just setting these parameters to be equal or vanishing in the quadratic χ^2 .

Since the uncertainties on the ϵ_i parameters are now smaller than 1, the universal approximation starts to be accurate. In the next sections, where we analyze several specific models, we will systematically compare our full numerical fit (plotting best fit regions in yellow with continuous contours at the 90 and 99% C.L.) with the universal approximation (best fit ellipsoidal regions in gray with dotted contours, at the same confidence levels).

5 Model-dependent Higgs fits

5.1 Higgs production cross sections

Assuming the SM predictions for the Higgs decays, we extract from the data the Higgs production cross sections. We find that they agree with SM predictions, as shown in fig. 3a. As expected, the most precisely probed cross section is the dominant one, $\sigma(pp \rightarrow h)$. At the opposite extremum $\sigma(pp \rightarrow jjh)$ is still largely unknown. The uncertainties on the reconstructed cross sections are correlated, although we do not report the correlation matrix.

5.2 Higgs couplings

We here extract from data the Higgs boson couplings to vectors and fermions, assuming that only the SM particles contribute to the $h \rightarrow gg, \gamma\gamma, \gamma Z$ loops. This amounts to restrict the universal fit in terms of the r_i parameters by setting the parameters for loop couplings to

$$r_g = r_t, \quad r_\gamma \approx 1.282r_W - 0.282r_t \quad r_{Z\gamma} \approx 1.057r_W - 0.057r_t \quad (14)$$

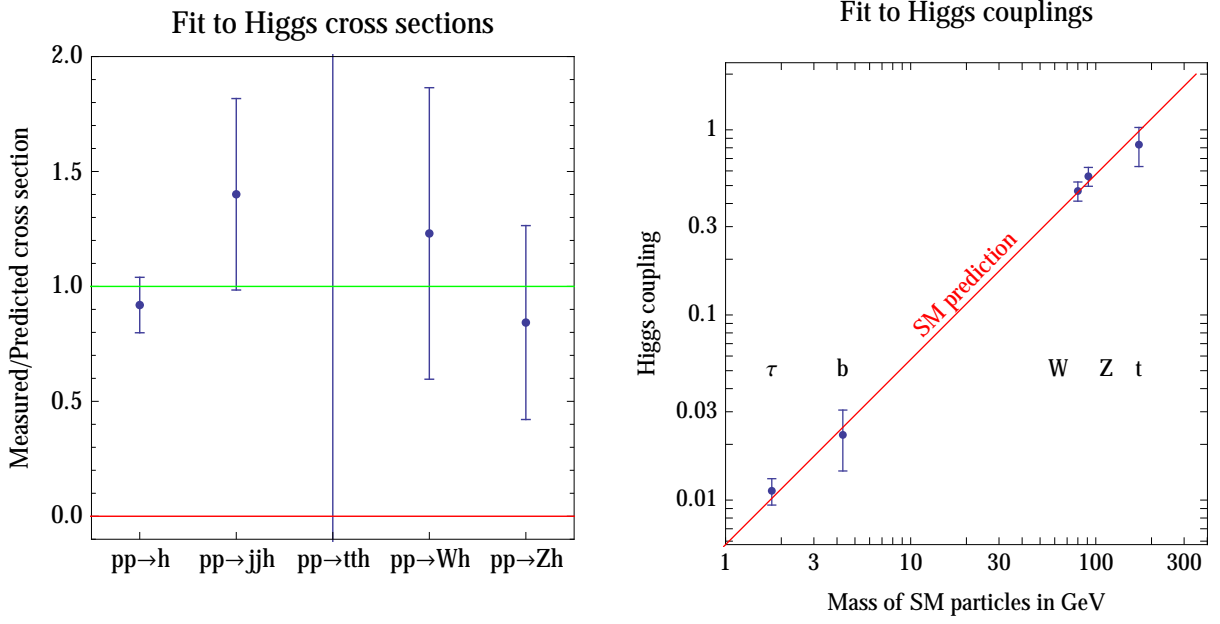


Figure 3: **Left:** reconstruction of the Higgs production cross sections in units of the SM prediction. **Right:** reconstruction of the Higgs couplings to the t, Z, W, b, τ , assuming that no new particles exist. The SM predicts that Higgs couplings are proportional to particle masses (diagonal line).

These numerical expressions are obtained by rescaling the expressions for the SM loops summarised in appendix A. In particular, the W loop (rescaled by r_W) and the top loop (rescaled by r_t) contribute to $h \rightarrow \gamma\gamma$ with a negative interference.

Under this assumption the top coupling of the Higgs, r_t , becomes indirectly probed via the loop effects. The fit to the couplings is shown in fig. 3a and agrees with the SM predictions, signalling that the new boson really is the Higgs. We do not report the correlation matrix, which can be immediately obtained by inserting eq. (14) into the universal χ^2 of eq. (12).

5.3 Composite Higgs models

Models where the Higgs is composite often assume the further restriction, in addition to eq. (14), of a common rescaling with respect to their SM values of the Higgs boson couplings to the W, Z bosons and a common rescaling of the Higgs boson couplings to all fermions. These rescalings are usually denoted as a and c , respectively:

$$r_t = r_b = r_\tau = r_\mu = c, \quad r_W = r_Z = a. \quad (15)$$

The resulting fit is shown in fig. 4a. We see that the best fit converged towards the SM; in particular data now disfavour the solution with $c < 0$ which appeared in previous fits and gave an enhanced $h \rightarrow \gamma\gamma$. We also see that our approximated universal fit (dotted contours) reproduces very well our full fit (continuous contours).

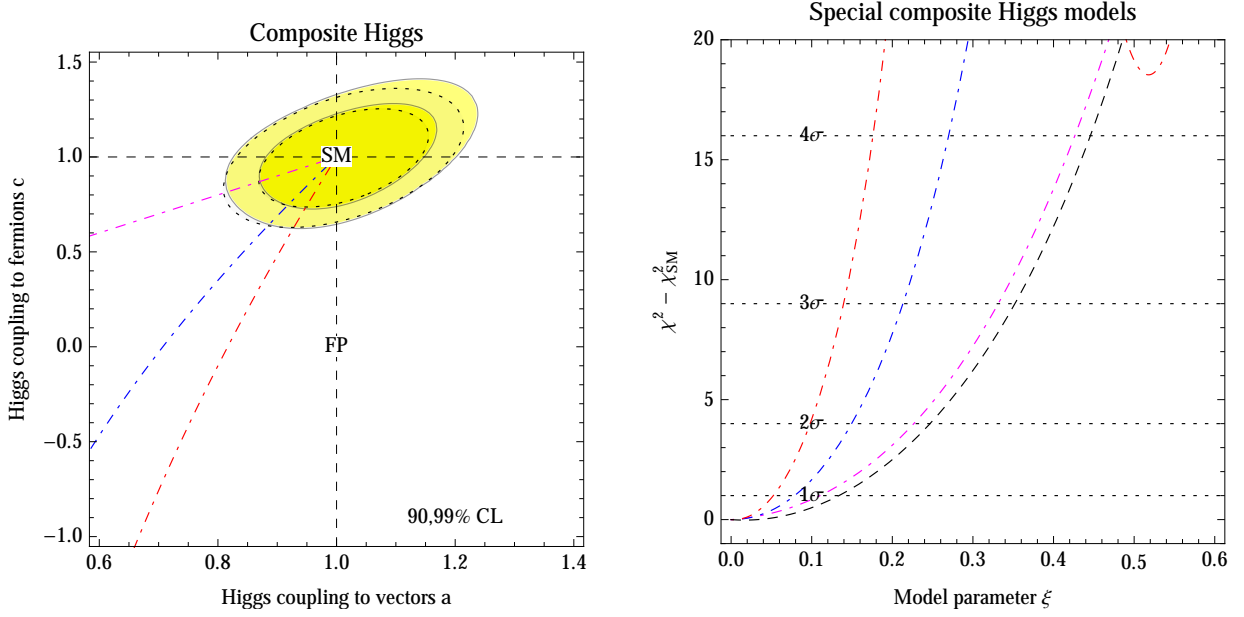


Figure 4: **Left:** fit of the Higgs boson couplings assuming common rescaling factors a and c with respect to the SM prediction for couplings to vector bosons and fermions, respectively. The two sets of contour lines are our full fit (continuous) and our approximated ‘universal’ fit (dotted). **Right:** values of the χ^2 along the trajectories in the (a, c) plane shown in the left panel, and given by $a = \sqrt{1-\xi}$ and $c = a$ (magenta) $c = (1 - 2\xi)/a$ (blue) $c = (1 - 3\xi)/a$ (red), as motivated by composite Higgs models. The black dashed curve corresponds to $a = 1$ and $c = 1 - \xi$.

In fig. 4b we show the full χ^2 restricted along the trajectories in the (a, c) plane (plotted in the left panel) predicted by simple composite pseudo-Goldstone Higgs models in terms of the parameter $\xi = (V/F_\pi)^2$, where F_π is the scale of global symmetry breaking.

5.4 New physics only in the loop processes

We here assume that only the loop processes are modified with respect to the SM predictions, summarized in appendix A. This amounts to restrict our universal fit setting

$$r_t = r_b = r_\tau = r_\mu = r_W = r_Z = 1, \quad \frac{\Gamma(h \leftrightarrow gg)}{\Gamma(h \leftrightarrow gg)_{\text{SM}}} = r_g^2, \quad \frac{\Gamma(h \rightarrow \gamma\gamma)}{\Gamma(h \rightarrow \gamma\gamma)_{\text{SM}}} = r_\gamma^2 \quad (16)$$

with $\text{BR}_{\text{inv}} = 0$ and $r_{Z\gamma} = 1$. The latter assumption is at present justified because of the large experimental error in the $h \rightarrow Z\gamma$ rate, even though in general new physics in the loop processes would induce deviation from unity in both $r_{Z\gamma}$ and r_γ . The result is shown in the left panel of fig. 5, under the form of a fit to the ratios of $\text{BR}(h \rightarrow gg)$ and $\text{BR}(h \rightarrow \gamma\gamma)$ with respect to the SM. One can see that the SM is well within the 1σ contour. The universal fit approximates well the full fit. The dashed trajectories show the loop effect due to extra scalar particles with the same quantum numbers of the top (red), of the bottom (blue), of the tau (vertical black line). The explicit expressions for the contribution of scalar, fermion and vector particles running

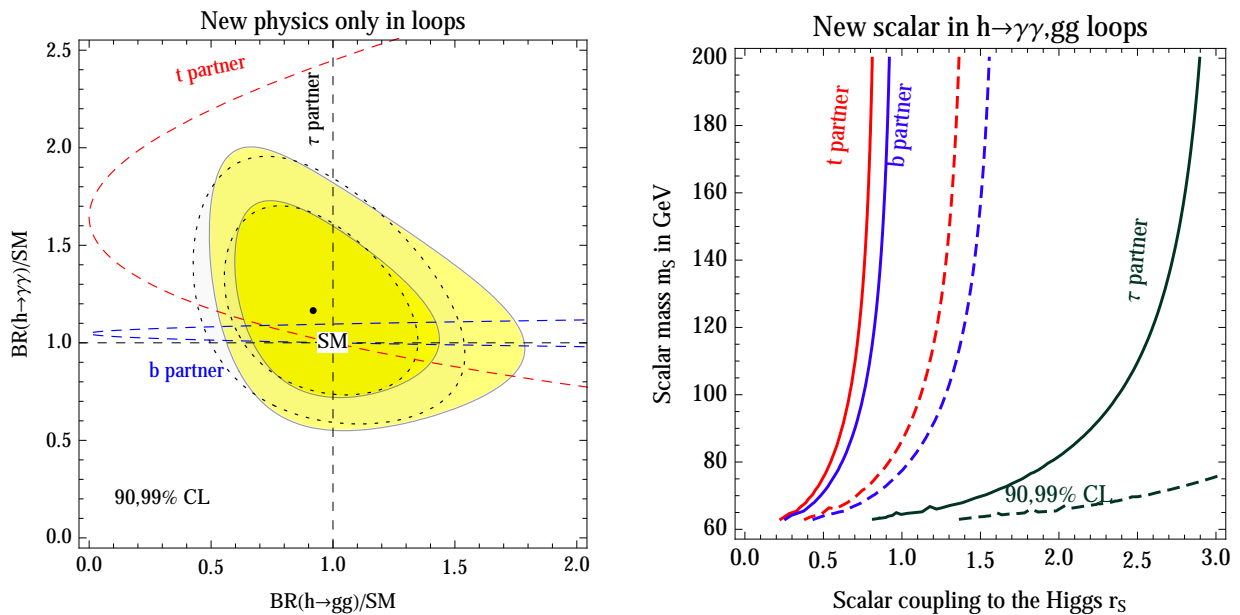


Figure 5: **Left:** fit for the Higgs boson branching fraction to photons and gluons, with 1 and 2σ contours. The dashed curves show the possible effect of extra scalar partners of the top (red), of the bottom (blue), of the tau (black). Dotted lines show the Gaussian approximation. **Right:** Upper bound at 90% (solid) and 99% (dashed) C.L. on the new scalar coupling r_S to the Higgs as a function of the new scalar mass m_S .

in the loop can be found in appendix A. Note that any additional color-less but electrically charged particle would lead to the same trajectory obtained for the scalar partner of the τ .

To better investigate the constraints on a possible new scalar S , in the right panel of fig. 5 we show the upper bound, as function of the scalar mass m_S , on the scalar coupling r_S to the Higgs boson, defined by the coupling

$$r_S \frac{2m_S^2}{V} hSS. \quad (17)$$

The resulting loop effects are summarised in appendix A. The solid and dashed curves in fig. 5b are respectively the upper bounds at 90% (solid) and 99% (dashed) C.L. More stringent limits are obtained on the top and bottom partners than on the τ partner.

One can also use the universal fit with the assumption of eq. (16) to derive indirect constraints on the top quark magnetic and chromomagnetic dipole moments [26, 27], which in the SM are expected to be respectively $g_t \approx 2$ and $k_t \approx 2$. Allowing g_t and k_t to vary freely, the $h \rightarrow \gamma\gamma$ and $h \rightarrow gg$ amplitudes are modified with respect to the SM according to:

$$r_\gamma = \frac{c_\gamma^{(W)} + c_\gamma^{(t)} \left(\frac{3}{8}g_t^2 - \frac{1}{2} \right)}{c_\gamma^{(W)} + c_\gamma^{(t)}}, \quad r_g = \frac{3}{8}k_t^2 - \frac{1}{2}, \quad (18)$$

where the quantities $c_\gamma^{(W)}$ and $c_\gamma^{(t)}$ are defined in eq. (33) of the Appendix. Fig. 6 shows the

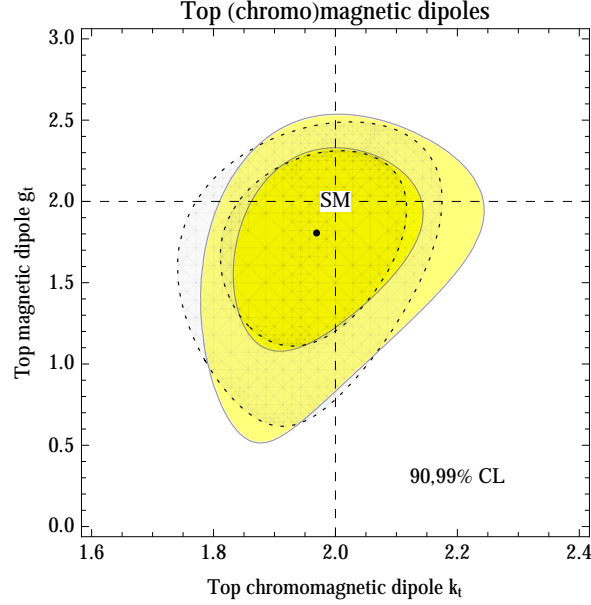


Figure 6: *Best fit regions for the (chromo)magnetic dipole moments of the top quark.*

90% and 99% C.L. allowed regions for g_t and k_t . The uncertainty on k_t is comparable to the one from its direct measurement, while the one for g_t is even smaller [28].

5.5 Models with two Higgs doublets

There are four types of two Higgs doublets models (2HDM) where tree level flavour-changing neutral currents (FCNCs) are forbidden by a Z_2 symmetry [35] and both doublets H_1 and H_2 get a vacuum expectation value:

- type I [36, 37] where only one doublet couples to all quarks and leptons;
- type II [37, 38], where up-type quarks couple to H_2 and H_1 couples to down-type quarks and leptons. The Higgs sector of the MSSM is a type II 2HDM;
- type X (lepton-specific or leptophilic) where H_2 couples only to quarks and H_1 couples only to leptons;
- type Y (flipped) [41], where H_2 couples to up-type quarks and H_2 to down-type quarks, and (contrary to the type II HDM) leptons couple to H_2 .

For an extensive review see [39] and for some previous fits see [40]. The modification to Yukawa couplings to up-type and down-type quarks and leptons in the four 2HDMs are:

	Type I	Type II	Type X (lepton-specific)	Type Y (flipped)
r_t	$\cos \alpha / \sin \beta$	$\cos \alpha / \sin \beta$	$\cos \alpha / \sin \beta$	$\cos \alpha / \sin \beta$
r_b	$\cos \alpha / \sin \beta$	$-\sin \alpha / \cos \beta$	$\cos \alpha / \sin \beta$	$-\sin \alpha / \cos \beta$
r_τ	$\cos \alpha / \sin \beta$	$-\sin \alpha / \cos \beta$	$-\sin \alpha / \cos \beta$	$\cos \alpha / \sin \beta$

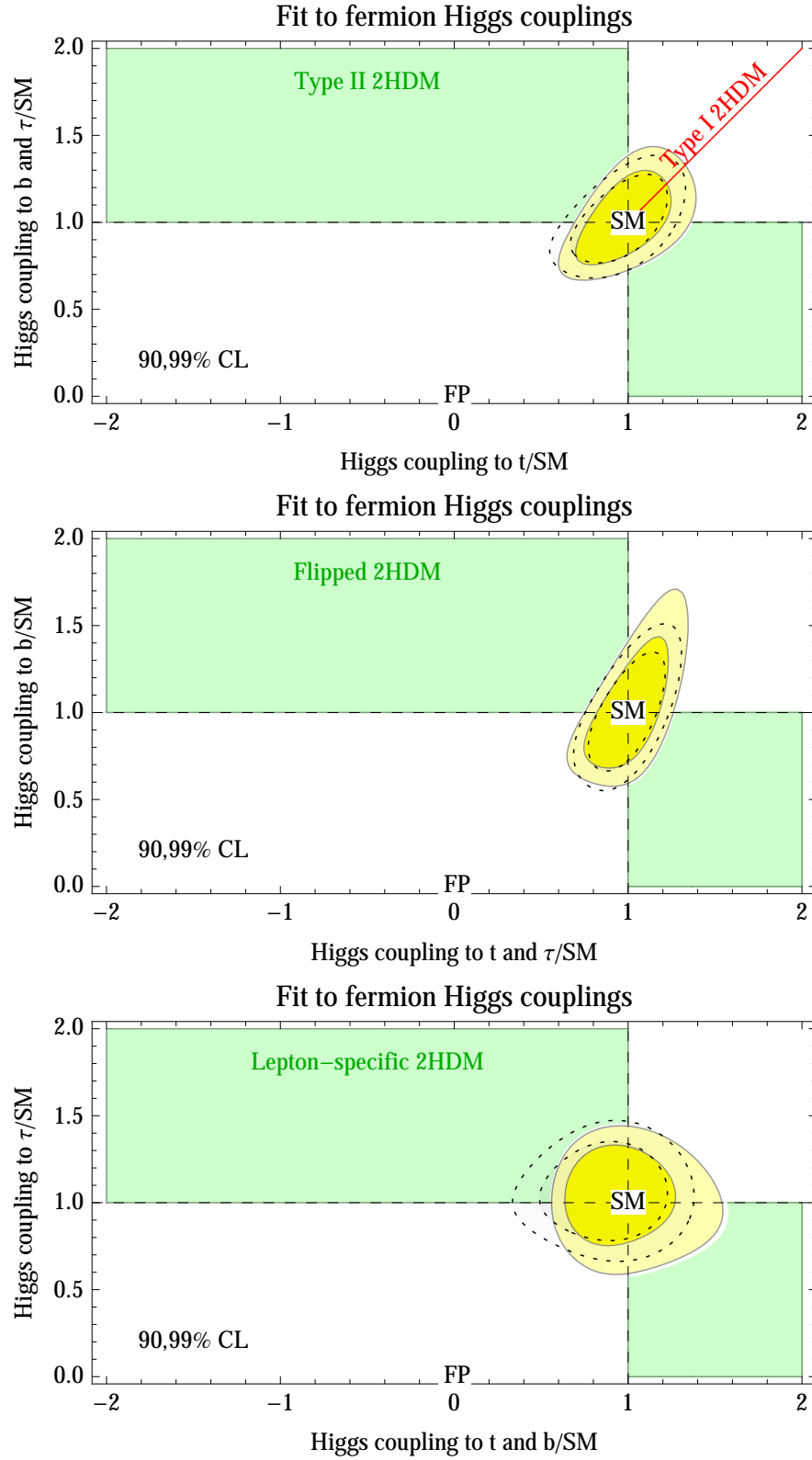


Figure 7: Fit to the t -quark and to b -quark and τ -lepton Yukawa couplings assuming the structure predicted by the various types of two Higgs doublet models. The point marked as ‘SM’ is the Standard Model; the point marked as ‘FP’ is the fermiophobic case.

As usual, $\tan \beta = v_2/v_1$ is the ratio of the VEVs of the two doublets and α is the mixing angle of the CP-even mass eigenstates. The SM limit corresponds to $\beta - \alpha = \pi/2$. In all of the models the vector couplings are also modified as

$$r_W = r_Z = \sin(\beta - \alpha). \quad (19)$$

The results of our fits are presented in fig. 7 in terms of the fermion couplings r_t, r_b, r_τ , restricted by the 2HDM models to lie within the green regions.

The type II 2HDM (upper panel) allows for independent modification of the t coupling r_t , and for a common modification of the b and τ couplings, $r_b = r_\tau$. The former is predicted be reduced and the latter enhanced by the model. The modification of eq. (19) of the vector couplings can be equivalently written as $r_W = r_Z = (1 + r_t r_b)/(r_t + r_b) \simeq 1 + \epsilon_t \epsilon_b/2$, showing that it is a small second order effect. In this model a negative t Yukawa coupling is still allowed at slightly more than 99% CL. The red line in the same panel shows the parameter space allowed by type I 2HDM, where all the couplings scale uniformly.

In the flipped 2HDM (middle panel) the τ Yukawa coupling changes in the same way as the t coupling and the region with negative coupling is disfavoured by data. Finally, in the leptophilic 2HDM (lower panel) the t and b couplings vary in the same way, while the τ coupling is independent.

The universal fit provides a good approximation to the full fit in all 2HD models.

5.6 Supersymmetry

Supersymmetry can affect Higgs physics in many different ways, such that it is difficult to make general statements. We here focus on the two most plausible effects:

- Stop loops can enhance or reduce the Higgs coupling to the top (and consequently the $h \leftrightarrow gg, \gamma\gamma, Z\gamma$ rates) by an amount given by

$$R_{\tilde{t}} = 1 + \frac{m_t^2}{4} \left[\frac{1}{m_{\tilde{t}_1}^2} + \frac{1}{m_{\tilde{t}_2}^2} - \frac{(A_t - \mu/\tan \beta)^2}{m_{\tilde{t}_1}^2 m_{\tilde{t}_2}^2} \right] \quad (20)$$

in the limit of heavy stop masses, $m_{\tilde{t}_{1,2}} \gg m_t$.

- The type II 2HDM structure of supersymmetric models modifies at tree level the Higgs couplings, as already discussed in section 5.5.

All of this amounts to specialise the universal χ^2 inserting the following values of its parameters

$$r_t = R_{\tilde{t}} \frac{\cos \alpha}{\sin \beta}, \quad r_b = r_\tau = r_\mu = -\frac{\sin \alpha}{\cos \beta}, \quad r_W = r_Z = \sin(\beta - \alpha). \quad (21)$$

Furthermore, the parameters $r_g, r_\gamma, r_{Z\gamma}$ relative to loop processes are fixed as in eq. (14). We trade the α parameter (mass mixing between Higgses) for the pseudo-scalar Higgs mass m_A using

$$\tan 2\alpha = \frac{m_A^2 + M_Z^2}{m_A^2 - M_Z^2} \tan 2\beta. \quad (22)$$

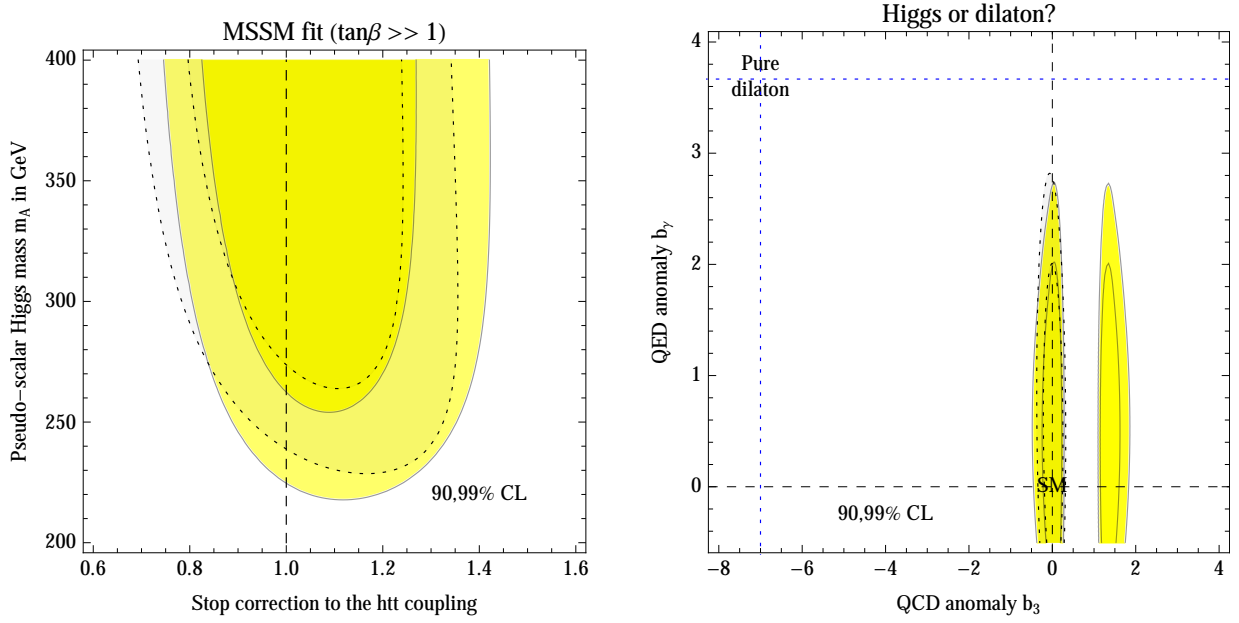


Figure 8: **Left:** Fit to the two main effects present in supersymmetry: stop loop correction to the $h t \bar{t}$ coupling and tree-level modification of the Higgs couplings due to the two-Higgs doublet structure. **Right:** fit as function of the β -function coefficients $b_3 = b_\gamma$ that parameterise dilaton models. The SM Higgs is reproduced at the experimentally favored point $b_3 = b_\gamma = 0$, while the pure dilaton is excluded at more than 5σ .

Finally, we assume a large $\tan \beta$, as motivated by the observed value of the Higgs mass. Fig. 8a shows the resulting fit. Once again, the universal fit approximates well the full fit. Of course, supersymmetry can manifest in extra ways not considered here, e.g. very light staus or charginos could enhance $h \rightarrow \gamma\gamma$ [31].

5.7 Data prefer the Higgs to the dilaton

As another example of a model where both the tree level and the loop level Higgs couplings are modified, we consider the dilaton. The dilaton is an hypothetical particle φ , that, like the Higgs, couples to SM particles with strength proportional to their masses [32]. More precisely the dilaton has a coupling to the trace of the energy-momentum tensor $T_{\mu\nu}$, suppressed by some unknown scale Λ :

$$\frac{\varphi}{\Lambda} T_\mu^\mu = \frac{\varphi}{\Lambda} \left(\sum_f m_f \bar{f} f - M_Z^2 Z_\mu^2 - 2M_W^2 W_\mu^2 + b_3 \frac{\alpha_3}{8\pi} G_{\mu\nu}^a G_{\mu\nu}^a + b_\gamma \frac{\alpha_{\text{em}}}{8\pi} F_{\mu\nu} F_{\mu\nu} \right). \quad (23)$$

The dilaton couplings to gg and $\gamma\gamma$ differ from the corresponding Higgs boson couplings, because eq. (23) contains the latter two quantum terms, that are present in T_μ^μ because scale invariance is anomalous and broken at quantum level by the running of the couplings. Indeed b_3 and b_γ are the β -function coefficients of the strong and electromagnetic gauge couplings. In the SM

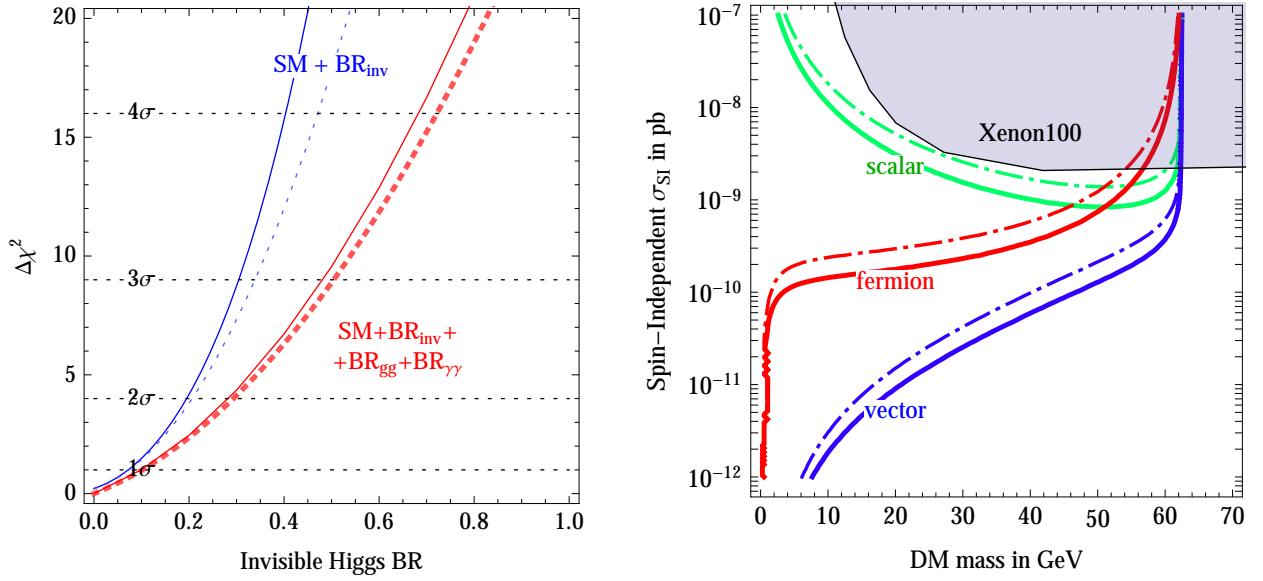


Figure 9: **Left:** fits to the invisible Higgs boson branching fraction under the two different assumptions described in section 5.8. The full fit (continuous curves) is well approximated by the universal fit (dotted curves). **Right:** upper limit on the spin-independent DM cross section on nucleons as a function of the DM mass for scalar (green), Majorana fermion (red) and vector (blue) DM. We adopted the 95% C.L. bounds $\text{BR}_{\text{inv}} < 0.19$ (solid, eq. (25)) and < 0.28 (dot-dashed, eq. (26)). The shaded region is excluded at 90% C.L. by XENON100 [25].

they have the explicit values $b_3 = -7$ and $b_\gamma = 11/3$: we call ‘pure dilaton’ this special model, which gives a significant enhancement of $h \leftrightarrow gg$.

Models where a dilaton arises usually often contain also new light particles, such that b_3 and b_γ can differ from their SM values. Thereby we perform a generic fit where b_3 and b_γ are free parameters in addition to Λ . Then, our universal fit is adapted to the case of the generic dilaton by setting

$$r \equiv r_W = r_Z = r_t = r_b = r_\tau = \frac{V}{\Lambda}, \quad r_g \approx r(1 - 1.45b_3), \quad r_\gamma \approx r(1 + 0.15b_\gamma) \quad (24)$$

where $V = 246 \text{ GeV}$.

In our previous analyses [8, 9], the dilaton gave fits of comparable quality to the SM Higgs, despite the significantly different predictions of the dilaton: enhanced $\gamma\gamma$ rates and reduced vector boson fusion rates. The first feature is no longer favoured by data, and the second feature is now disfavoured: so we find that present data prefer the Higgs to the ‘pure dilaton’ at about 5σ level. We then consider the generic dilaton, showing in fig. 8b that the allowed part of its parameters space is the one where it mimics the Higgs, possibly up to a sign difference in r_g and/or r_γ . The dilaton becomes identical to the SM Higgs in the limit $b_3 = b_\gamma = 0$ and $\Lambda = V$. This situation is not easily realisable in models, given that adding extra charged particles increases b_γ rather than reducing it.

5.8 Higgs boson invisible width

Next, we allow for a Higgs boson invisible width, for example into Dark Matter. We perform two fits.

1. In the first fit, the invisible Higgs width is the only new physics. We find (blue curves in fig. 9a) that present data imply

$$\text{BR}_{\text{inv}} = -0.08 \pm 0.16 \quad \text{i.e.} \quad \text{BR}_{\text{inv}} < 0.19 \text{ at 95\% C.L.}, \quad (25)$$

2. In addition to the invisible width we also allow for non-standard values of $h \rightarrow \gamma\gamma$ and $h \rightarrow gg$, finding a weaker constraint on BR_{inv} (red curves in fig. 9a)

$$\text{BR}_{\text{inv}} < 0.28 \text{ at 95\% C.L.} \quad (26)$$

Notice that the main constraint on BR_{inv} does not come from the direct search for $pp \rightarrow Zh \rightarrow \ell\ell\cancel{E}_T$ (included in our data-set) but from the global fit [8, 33].

5.9 Dark Matter models

The invisible Higgs boson decay width [33] constrains Dark Matter (DM) candidates with mass below $M_h/2$. The Higgs sector of the SM allows for a direct coupling to particles of a hidden sector. If the latter are stable and interact weakly with the SM sector, they could represent viable Dark Matter (DM) candidates. If DM particles have mass below $M_h/2$, the Higgs boson can thus decay into a couple of DM particles, which would escape detection. Invisible Higgs decays are constrained by the fact that the ATLAS and CMS Higgs rates are compatible with the predictions of the SM Higgs boson. The experimental bound on BR_{inv} can be used to constrain the DM mass and its elastic cross section on nucleons probed in direct detection experiments, as illustrated for instance in [24], where DM is assumed to be either a scalar S , or a Majorana fermion f or a vector V coupled to the Higgs as

$$r_S \frac{2m_S^2}{V} hSS + r_f \frac{m_f}{V} h\bar{f}f + r_V \frac{2m_V^2}{V} hV_\mu V_\mu. \quad (27)$$

The partial Higgs decay width into dark matter $\Gamma(h \rightarrow \text{DM DM})$ and the spin-independent DM-proton elastic cross section σ_{SI} can be calculated in terms of the parameters of the above Lagrangian. Both are proportional to the square of the DM-Higgs coupling, so that the ratio $\mu \equiv \sigma_{\text{SI}}/\Gamma(h \rightarrow \text{DM DM})$ depends only on the unknown DM mass and on the known masses and couplings of the relevant SM particles (see for instance the expressions provided in [24]).

This allows us to relate the invisible Higgs branching fraction to the DM direct detection cross section:

$$\text{BR}_{\text{inv}} \equiv \frac{\Gamma(h \rightarrow \text{DM DM})}{\Gamma_h^{\text{SM}} + \Gamma(h \rightarrow \text{DM DM})} = \frac{\sigma_{\text{SI}}}{\mu \Gamma_h^{\text{SM}} + \sigma_{\text{SI}}} \quad (28)$$

where $\Gamma_h^{\text{SM}} = 4.1 \text{ GeV}$ is the total Higgs decay width into all SM particles, that we fix to its SM prediction. For a given DM mass, an upper bound on the Higgs invisible branching fraction implies an upper bound on the DM scattering cross section on nucleons. The relation between

the invisible branching fraction and the direct detection cross section strongly depends on the spinorial nature of the DM particle, in particular, the strongest (weakest) bound is derived in the vectorial (scalar) case.

Imposing the upper bounds on BR_{inv} derived in section 5.8, fig. 9 shows the corresponding upper limits on the spin-independent DM cross section on nucleons as a function of the DM mass, in the case of scalar (green), Majorana fermion (red) and vector (blue) DM candidates.

In all cases, the derived bounds are stronger than the direct one from XENON100 as long as the mass of DM is lighter than $M_h/2$. This conclusion does not rely on the assumption that DM is a thermal relic that reproduces the observed cosmological DM abundance.

6 Discussion and Conclusions

The LHC experiments reported their measurements of Higgs boson properties at the Moriond 2013 conferences, based on the full collected luminosity during 2011 and 2012. At the same time, TeVatron reported their final Higgs results. With the crucial inclusion of the full CMS $\gamma\gamma$ data (missing in previous analyses), at this stage all main Higgs results from TeVatron and from the first phase of LHC have been basically presented. Those results will drive our understanding of particle physics, until new 13 TeV LHC data will be available.

Motivated by these results, we have performed a state-of-the-art global fit to Higgs boson data, including all sub-categories studied by the experimental collaborations, for a total of 56 data-points, as summarised in fig. 1. We found that the average Higgs rate is 1.00 ± 0.10 in SM units, supporting the SM Higgs boson hypothesis. The Higgs boson mass is usually determined from the peaks in the invariant mass distribution of ZZ and $\gamma\gamma$. We performed the first measurement of the Higgs boson mass from the rates, finding that the two determinations are compatible:

$$M_h = \begin{cases} 125.66 \pm 0.34 \text{ GeV} & \text{from the peaks,} \\ 124.2 \pm 1.8 \text{ GeV} & \text{from the rates.} \end{cases} \quad (29)$$

The LHC physics program has been successful: with only $\approx 25/\text{fb}$ of data per experiment the Higgs boson has been discovered and several of its properties determined within $\approx \pm 20\%$ precision. We are now entering into the era of precision Higgs physics — deviations from the SM due to new physics no longer can dominate the data. This observation allowed us to propose a ‘universal’ form in which experiments could report their results allowing theorists to easily test any desired model. The new assumption that makes possible this significant simplification is that new physics is a small correction to the SM. While we present our own global combination in ‘universal’ form in eq. (13), we stress that only the experimental collaborations can perform a fully precise analysis.

We studied several new physics scenarios beyond the SM. We determined from data the production cross sections (assuming standard Higgs decays) and the Higgs decays widths (assuming standard productions), finding that they lie along the SM predictions. In a more general context, we allowed all possible Higgs boson couplings to any SM particle to deviate from its SM value, finding that couplings to the W, Z, t, b, τ must lie around their SM predictions up to

uncertainties of about $\pm 20\%$ (see fig. 3b). In particular, non-standard Higgs boson couplings to vectors, predicted by composite Higgs models, are most stringently constrained. The scenario of negative Higgs coupling to fermions (‘dysfermiophilia’) that gave the best fit with early LHC data is now disfavoured at more than 2σ .

We considered various specific new physics models: new scalars, 2HDM, supersymmetry, dilaton, composite Higgs, invisible Higgs decays, possibly into Dark Matter particles, anomalous couplings of the top, etc. The results of those fits are presented in numerous figures throughout the paper. Qualitatively, all reach to the same conclusions:

- i) best fit regions lie along SM predictions, imposing constraints on new physics;
- ii) our simple ‘universal’ approximation to the full fit is adequate.

In particular we find that, with the latest data, the dilaton alternative to the Higgs is now excluded at 5σ , with the exception of the special non-minimal dilaton tuned to exactly reproduce the Higgs (section 5.7).

We will update this paper at the light of future results.

Acknowledgement This work was supported by the ESF grants 8943, MTT8, MTT59, MTT60, MJD140 by the recurrent financing SF0690030s09 project and by the European Union through the European Regional Development Fund. The work of P. P. G. has been partially funded by the “Fondazione A. della Riccia”.

A New physics contributions to loop processes

The coefficients in the second line of eq. (7) arise at one-loop. They are obtained by summing the contributions of all scalars (S) fermions (f) and vectors (V) that couple to the Higgs as in eq. (27). The explicit expressions for the loop effects are [29]:

$$\begin{aligned} c_g^{(S)} &= \frac{C_2^S}{2} r_S A_S(\tau_S) & c_g^{(f)} &= 2C_2^f r_f A_f(\tau_f) \\ c_\gamma^{(S)} &= \frac{N_S Q_S^2}{24} r_S A_S(\tau_S) & c_\gamma^{(f)} &= \frac{N_f Q_f^2}{6} r_f A_f(\tau_f) & c_\gamma^{(V)} &= -\frac{7Q_V^2}{8} r_V A_V(\tau_V) \end{aligned} \quad (30)$$

where for each particle $p = S, f, V$, $\tau_p = m_h^2/4m_p^2$, N_p is the number of colors, C_2^p is the Casimir of the color representation ($\text{Tr}(T^a T^b) = C_2 \delta^{ab}$), and the loop functions are

$$A_S(\tau) = \frac{3}{\tau^2} [f(\tau) - \tau] , \quad A_f(\tau) = \frac{3}{2\tau^2} [(\tau - 1)f(\tau) + \tau] \quad (31)$$

$$A_V(\tau) = \frac{1}{7\tau^2} [3(2\tau - 1)f(\tau) + 3\tau + 2\tau^2] \quad (32)$$

with $f(\tau) = \arcsin^2(\sqrt{\tau})$ for $\tau \leq 1$ such that $A_p(\tau_p) \rightarrow 1$ in the limit $\tau_p \rightarrow 0$ (heavy p -particle).

In particular, in the SM, the hgg coupling is dominated by the top loop, and the $h\gamma\gamma$ coupling arise from the sum of the top and W boson loops:

$$c_{\text{SM}}^{gg} = c_g^{(t)} = A_f(\tau_t) \quad c_{\text{SM}}^{\gamma\gamma} = c_\gamma^{(t)} + c_\gamma^{(W)} = \frac{2}{9} A_f(\tau_t) - \frac{7}{8} A_V(\tau_W) . \quad (33)$$

Beyond the SM (BSM) physics affects the parameters r_g and r_γ as

$$r_g = 1 + \frac{c_{\text{BSM}}^{gg}}{c_{\text{SM}}^{gg}}, \quad r_\gamma = 1 + \frac{c_{\text{BSM}}^{\gamma\gamma}}{c_{\text{SM}}^{\gamma\gamma}}. \quad (34)$$

For example, additional scalar particles with the same quantum numbers of a stop, sbottom and stau respectively contribute to c_{BSM}^{gg} and to $c_{\text{BSM}}^{\gamma\gamma}$ as:

$$\begin{aligned} c_g^{(\tilde{t})} &= \frac{1}{4} r_{\tilde{t}} A_S(\tau_{\tilde{t}}) & c_g^{(\tilde{b})} &= \frac{1}{4} r_{\tilde{b}} A_S(\tau_{\tilde{b}}) & c_g^{(\tilde{\tau})} &= 0 \\ c_\gamma^{(\tilde{t})} &= \frac{1}{18} r_{\tilde{t}} A_S(\tau_{\tilde{t}}) & c_\gamma^{(\tilde{b})} &= \frac{1}{72} r_{\tilde{b}} A_S(\tau_{\tilde{b}}) & c_\gamma^{(\tilde{\tau})} &= \frac{1}{24} r_{\tilde{\tau}} A_S(\tau_{\tilde{\tau}}). \end{aligned} \quad (35)$$

References

- [1] ATLAS Collaboration, Phys. Lett. B 716 (2012) 1 [[arXiv:1207.7214](#)].
- [2] CMS Collaboration, Phys. Lett. B 716 (2012) 30 [[arXiv:1207.7235](#)].
- [3] F. Englert and R. Brout, Phys. Rev. Lett. 13, 321 (1964).
- [4] P. W. Higgs, Phys. Lett. 12 (1964) 132.
- [5] P. W. Higgs, Phys. Rev. Lett. 13, 508 (1964).
- [6] G. S. Guralnik, C. R. Hagen and T. W. B. Kibble, Phys. Rev. Lett. 13, 585 (1964).
- [7] D. Carmi, A. Falkowski, E. Kuflik and T. Volansky, [arXiv:1202.3144](#). A. Azatov, R. Contino and J. Galloway, [arXiv:1202.3415](#). J. R. Espinosa, C. Grojean, M. Muhlleitner and M. Trott, [arXiv:1202.3697](#). T. Li, X. Wan, Y. Wang and S. Zhu, [arXiv:1203.5083](#). J. Ellis and T. You, [arXiv:1204.0464](#). A. Azatov, R. Contino, D. Del Re, J. Galloway, M. Grassi and S. Rahatlou, JHEP 1206 (2012) 134 [[arXiv:1204.4817](#)]. M. Klute, R. Lafaye, T. Plehn, M. Rauch and D. Zerwas, [arXiv:1205.2699](#); A. Azatov, S. Chang, N. Craig and J. Galloway, Phys. Rev. D 86 (2012) 075033 [[arXiv:1206.1058](#)]. I. Low, J. Lykken and G. Shaughnessy, Phys. Rev. D 86 (2012) 093012 [[arXiv:1207.1093](#)]. T. Corbett, O. J. P. Eboli, J. Gonzalez-Fraile and M. C. Gonzalez-Garcia, Phys. Rev. D 86 (2012) 075013 [[arXiv:1207.1344](#)]. M. R. Buckley and D. Hooper, Phys. Rev. D 86 (2012) 075008 [[arXiv:1207.1445](#)]. M. Montull and F. Riva, JHEP 1211 (2012) 018 [[arXiv:1207.1716](#)]. J. R. Espinosa, C. Grojean, M. Muhlleitner and M. Trott, [arXiv:1207.1717](#). D. Carmi, A. Falkowski, E. Kuflik, T. Volansky and J. Zupan, JHEP 1210 (2012) 196 [[arXiv:1207.1718](#)]. S. Banerjee, S. Mukhopadhyay and B. Mukhopadhyaya, JHEP 1210 (2012) 062 [[arXiv:1207.3588](#)]. D. Bertolini and M. McCullough, JHEP 1212 (2012) 118 [[arXiv:1207.4209](#)]. F. Bonnet, T. Ota, M. Rauch and W. Winter, Phys. Rev. D 86 (2012) 093014 [[arXiv:1207.4599](#)]. T. Plehn and M. Rauch, Europhys. Lett. 100 (2012) 11002 [[arXiv:1207.6108](#)]. J. R. Espinosa, C. Grojean, V. Sanz and M. Trott, [arXiv:1207.7355](#). A. Djouadi, [arXiv:1208.3436](#). G. Cacciapaglia, A. Deandrea, G. D. La Rochelle and J. -B. Flament, [arXiv:1210.8120](#). G. Moreau, [arXiv:1210.3977](#). G. Belanger, B. Dumont, U. Ellwanger, J. F. Gunion and S. Kraml, JHEP 1302 (2013) 053. E. Masso and V. Sanz, [arXiv:1211.1320](#). T. Corbett, O. J. P. Eboli, J. Gonzalez-Fraile and M. C. Gonzalez-Garcia, Phys. Rev. D 87 (2013) 015022 [[arXiv:1211.4580](#)]. C. Cheung, S. D. McDermott and K. M. Zurek, [arXiv:1302.0314](#). K. Cheung, J. S. Lee and P. -Y. Tseng, [arXiv:1302.3794](#). A. Falkowski, F. Riva and A. Urbano, [arXiv:1303.1812](#).
- [8] P. P. Giardino, K. Kannike, M. Raidal and A. Strumia, JHEP 1206 (2012) 117 [[arXiv:1203.4254](#)].
- [9] P. P. Giardino, K. Kannike, M. Raidal and A. Strumia, [[arXiv:1207.1347](#)].
- [10] LHC Higgs Cross Section Working Group, [arXiv:1101.0593](#) ([Recommended values on SM Higgs XS at 7 TeV](#)) and [arXiv:1201.3084](#) ([Branching Ratios and Partial-Decay Widths](#)).

- [11] Guillermo Gomez-Ceballos, CMS Collaboration, [Talk at the Moriond 2013 EW session](#).
- [12] Fabrice Hubaut, ATLAS Collaboration, [Talk at the Moriond 2013 EW session](#). Eleni Mountricha, ATLAS Collaboration, [Talk at the Moriond 2013 QCD session](#).
- [13] Valentina Dutta, CMS Collaboration, [Talk at the Moriond 2013 EW session](#). Victoria Martin, ATLAS Collaboration, [Talk at the Moriond 2013 EW session](#). ATLAS Collaboration, [ATLAS-CONF-2012-161](#).
- [14] Lidija Živković, CDF and DO Collaborations, [Talk at the Moriond 2013 EW session](#).
- [15] Christophe Ochoa, CMS Collaboration, [Talk at the Moriond 2013 QCD session](#). ATLAS Collaboration, [ATLAS-CONF-2013-012](#)
- [16] CMS Collaboration, [CMS-PAS-HIG-13-002](#). ATLAS Collaboration, [ATLAS-CONF-2013-013](#).
- [17] CMS Collaboration, [CMS-PAS-HIG-13-003](#). ATLAS Collaboration, [ATLAS-CONF-2013-030](#).
- [18] ATLAS Collaboration, [ATLAS-CONF-2012-160](#).
- [19] ATLAS Collaboration, [ATLAS-CONF-2012-161](#).
- [20] ATLAS Collaboration, [ATLAS-CONF-2013-010](#).
- [21] CMS Collaboration, [CMS-PAS-HIG-13-006](#). ATLAS Collaboration, [ATLAS-CONF-2013-009](#).
- [22] Mingshui Shen, CMS Collaboration, [Talk at the Moriond 2013 EW session](#). Bruno Mansoulie, CMS Collaboration, [Talk at the Moriond 2013 EW session](#). ATLAS Collaboration, [ATLAS-CONF-2013-014](#).
- [23] ATLAS Collaboration, [ATLAS-CONF-2013-011](#)
- [24] A. Djouadi, A. Falkowski, Y. Mambrini and J. Quevillon, [arXiv:1205.3169](#).
- [25] XENON100 Collaboration, Phys. Rev. Lett. 109 (2012) 181301 [[arXiv:1207.5988](#)].
- [26] L. Labun and J. Rafelski, [arXiv:1209.1046](#).
- [27] L. Labun and J. Rafelski, [arXiv:1210.3150](#).
- [28] J. F. Kamenik, M. Papucci and A. Weiler, Phys. Rev. D 85 (2012) 071501 [[arXiv:1107.3143](#)].
- [29] For a recent review see A. Djouadi, Phys. Rept. 457 (2008) 1 [[hep-ph/0503172](#)].
- [30] ATLAS collaboration, [ATLAS-CONF-2013-011](#). See also A. Djouadi, A. Falkowski, Y. Mambrini and J. Quevillon, [arXiv:1205.3169](#).
- [31] See e.g. M. Carena, I. Low and C. E. M. Wagner, JHEP 1208 (2012) 060 [[arXiv:1206.1082](#)]. G. F. Giudice, P. Paradisi, A. Strumia and A. Strumia, JHEP 1210 (2012) 186 [[arXiv:1207.6393](#)].
- [32] L. Randall and R. Sundrum, Phys. Rev. Lett. 83 (1999) 3370. Y. Eshel, S. J. Lee, G. Perez and Y. Soreq, JHEP 1110 (2011) 015 [[arXiv:1106.6218](#)]; V. Barger and M. Ishida, [arXiv:1110.6452](#). K. Cheung and T. -C. Yuan, Phys. Rev. Lett. 108 (2012) 141602 [[arXiv:1112.4146](#)].
- [33] J. R. Espinosa, M. Muhlleitner, C. Grojean and M. Trott, [arXiv:1205.6790](#). G. Belanger, B. Dumont, U. Ellwanger, J. F. Gunion and S. Kraml, [arXiv:1302.5694](#).
- [34] J. F. Gunion, H. E. Haber, G. L. Kane and S. Dawson, Front. Phys. 80 (2000) 1.
- [35] S. L. Glashow and S. Weinberg, Phys. Rev. D 15 (1977) 1958.
- [36] H. E. Haber, G. L. Kane and T. Sterling, Nucl. Phys. B 161 (1979) 493.
- [37] L. J. Hall and M. B. Wise, Nucl. Phys. B 187 (1981) 397.
- [38] J. F. Donoghue and L. F. Li, Phys. Rev. D 19 (1979) 945.
- [39] G. C. Branco, P. M. Ferreira, L. Lavoura, M. N. Rebelo, M. Sher and J. P. Silva, Phys. Rept. 516 (2012) 1 [[arXiv:1106.0034](#)].
- [40] R. T. D'Agnolo, E. Kuflik and M. Zanetti, [arXiv:1212.1165](#). A. Celis, V. Ilisie and A. Pich, [arXiv:1302.4022](#).
- [41] V. D. Barger, J. L. Hewett and R. J. N. Phillips, Phys. Rev. D 41 (1990) 3421. Y. Grossman, Nucl. Phys. B 426 (1994) 355 [[hep-ph/9401311](#)]. A. G. Akeroyd and W. J. Stirling, Nucl. Phys. B 447 (1995) 3. A. G. Akeroyd, Phys. Lett. B 377 (1996) 95 [[hep-ph/9603445](#)]. A. G. Akeroyd, J. Phys. G 24 (1998) 1983 [J. Phys. G 24 (1998) 1983] [[hep-ph/9803324](#)]. M. Aoki, S. Kanemura, K. Tsumura and K. Yagyu, Phys. Rev. D 80 (2009) 015017 [[arXiv:0902.4665](#)].
- [42] M. Carena, I. Low and C. E. M. Wagner, [arXiv:1206.1082](#). L. Wang and X. -F. Han, [arXiv:1206.1673](#). W. -F. Chang, J. N. Ng and J. M. S. Wu, [arXiv:1206.5047](#). N. Bonne and G. Moreau, [arXiv:1206.3360](#). B. Bellazzini, C. Petersson and R. Torre, [arXiv:1207.0803](#). J. Baglio, A. Djouadi and R. M. Godbole, [arXiv:1207.1451](#).